Design of an industrial multi-bed (V)PSA unit for argon concentration

Design of an industrial multi-bed (V)PSA unit for argon concentration

Mauro Luberti*, Hyungwoong Ahn

Institute for Materials and Processes, School of Engineering, The University of Edinburgh, Robert Stevenson Road, Edinburgh EH9 3FB, United Kingdom
corresponding author: m.luberti@ed.ac.uk

Abstract

Pressure swing adsorption systems have been devised to concentrate argon from a binary gas mixture of oxygen and argon (O_2:Ar = 95:5 mol%) that an industrial oxygen generation vacuum swing adsorption (VSA) unit produces from air. The kinetically-driven adsorption processes investigated in this study contain a self-purging step and up to two double-ended pressure equalization steps. Three adsorption cycle configurations, each of which has one, two and three beds, were simulated. The effects of pressure ranges of the adsorption cycle, either pressure swing adsorption (PSA, 1–3 bar) or vacuum swing adsorption (VSA, 0.1–1 bar), as well as adsorption step time were extensively assessed with respect to the following separation key performance indicators (KPIs): argon purity, argon recovery, bed productivity and specific energy consumption. It turned out that argon purity and recovery could be significantly improved in the VSA cycles at the expense of bed productivity and energy consumption. The single VSA unit could not concentrate argon up to a purity of 98+% which is typically required for certain applications such as steel production and inert gas welding. Thus, a second VSA unit was added to increase further the argon purity and it was found that the integrated two-stage VSA system is capable of achieving the following overall performances: argon purity of 98.1%, argon recovery of 20.3%, bed productivity of 0.011 $mol_{Ar}\ kg_{ads}^{-1}\ h^{-1}$ and specific energy consumption of 53.2 MJ kg_{Ar}^{-1}. Considering real efficiencies of turbomachinery the energy consumption of the proposed VSA unit resulted 75% higher than that of a conventional stand-alone cryogenic distillation system designed to achieve the same separation. However, the VSA technology is expected to be a more attractive option than the cryogenic process in terms of CAPEX.

***Keywords**: Argon, Vacuum Pressure Swing Adsorption, Multi-bed PSA, Energy Consumption, Cryogenic Distillation, Process Simulation*

1. Introduction

After nitrogen and oxygen, argon is the most abundant component in air with a concentration of 0.93% by volume or 1.25% by weight. Soon after the world's first air separation plant using the double-column rectification process was installed, argon started to be coproduced in 1913 [1] and its production has increased dramatically over the years. Argon has been extensively used in various industries, such as steel production, inert gas welding, incandescent lamps, silicon crystal growth and wine preservation [2–5].

Multi-column cryogenic distillation of air is currently the most efficient technology for producing large quantities of oxygen, nitrogen and argon as gaseous or liquid products with high purities and recoveries [6]. As argon concentration is at its maximum in the lower portion of the low-pressure column (argon belly), a vapour side-draw containing about 10-12% of argon is normally drawn off at this section and sent to a crude argon superstaged column. In modern air separation plants high purity, oxygen-free argon can be produced directly by this superstaged distillation process or, alternatively, the crude argon purity can be further refined by a catalytic combustion system employing hydrogen [7,8] or a cryogenic adsorption system with zeolite molecular sieves [9]. A lot of researches have focused for the last three decades on trying to improve the energy efficiency associated to cryogenic air separation units (ASUs) [10–13] or integrated systems of cryogenic ASUs and adsorption processes including PSA, VSA, Duplex PSA, and TSA [4,8,14,15]. However, despite the efforts, cryogenic distillation technology is doomed to be highly energy intensive as the system needs to be kept in a temperature range between -180°C and -150°C. Accordingly, it has been reported that a conventional ASU incurs a specific energy consumption of 280–460 kWh t_{O2}^{-1} [13,16]. Given the close boiling points of oxygen and argon, a typical superstaged column often exceeds 60 m in height to attain a high purity argon. As a consequence, considerable capital expenditure (CAPEX) is required for the cryogenic system to include split columns, multiple coldbox sections and liquid reflux pumps [15]. Catalytic combustion systems necessitate hydrogen which is not always readily available in a cost effective way over the world. Cryogenic adsorption systems present the issue of quick cooling to cryogenic temperatures immediately after the high temperature desorption step [14].

On the other hand adsorption-based processes have also recently expanded their share in air separation industry, given their superior performances in small-to-medium scale applications. Compared to cryogenic distillation, adsorption technology is a better option due to its easier operation, reduced maintenance and lower energy consumption [17,18]. A vacuum swing adsorption using zeolites is employed to produce oxygen from air but it is well known that the maximum achievable concentration of oxygen in the product is limited to 95 mol% [19]. At this purity the remaining component in the product gas is mostly argon because argon and oxygen exhibit very similar adsorption equilibrium properties relative to nitrogen on typical commercially-available zeolite adsorbents [20]. Since this raffinate gas is not suitable for several industrial applications that require an oxygen purity of 99+%, it has been

sought to purify the crude oxygen gas by removing argon via kinetic separations, as exemplified in research papers [21–23] and patents [24–26].

At the same time a technically simple and cost-effective pressure swing adsorption process can also be developed to produce a high purity of argon from this oxygen-rich stream. So far, there are very few studies published in literature tackling this separation using adsorption technology. At ambient temperature little or no equilibrium selectivity for oxygen over argon is observed with common adsorbents. Instead, kinetically-controlled PSA processes using carbon molecular sieves (CMS) [27–29] or titanosilicate molecular sieves [20] have been proposed for this separation. Hayashi et al. [3] devised a five-stage lab-scale PSA process to obtain highly concentrated argon and high purity oxygen from air simultaneously. The first, fourth and fifth stages comprised three 5A zeolite columns to remove nitrogen impurity while the second and third stages comprised two and three columns, respectively, packed with 3A carbon molecular sieve to separate oxygen and argon. By configuring the cycles with a maximum pressure swing between 0.13 bar and 3.5 bar and employing an intermediate catalytic deoxygenation unit, it was claimed that this process could concentrate argon to a purity of 99%. Thanks also to recycled streams, the argon was recovered with a 40% yield from the second- to the fifth-stage PSA apparatus. Rege and Yang [30] assessed the feasibility of producing high purity argon from a mixture of 95% O_2 and 5% Ar using VSA cycles with Bergbau-Forschung CMS. A two-bed five-step cycle with an intermediate co-current blowdown step was simulated considering an adsorption pressure of 1.0 atm and a desorption pressure of 0.2 atm. It was shown that with a co-current depressurization pressure of 0.9 atm argon could be concentrated up to a purity of 87% but with a recovery as low as 14.9%. Jin et al. [31] compared four adsorbents for the kinetically-controlled separation of argon from a 95:5 mol% oxygen-argon mixture. They concluded that Takeda II CMS showed the highest selectivity of O_2 over Ar and used this adsorbent to carry out lab-scale PSA experiments involving a single-bed three-step cycle. After validating the PSA simulation model with the above experiments, several parameters were systematically evaluated on the PSA performance including cycle step times, ratio of column length to feed velocity and lowest operating pressure. It was observed that for the PSA runs the maximum argon purity was 50.1% with a recovery of 38.7% while for the VSA runs the maximum argon purity was around 80% with a recovery of 43%.

It is clear from the previous studies that one-stage kinetically-driven (V)PSA process is not sufficient to concentrate argon to a purity which is typically required for certain applications such as steel production and inert gas welding. Besides, it is also fundamental to minimize the overall number of adsorption beds and separation stages in order to minimize the unit CAPEX. The objective of this work is to design a cost-effective industrial pressure swing adsorption unit capable of producing argon with a purity of 98+%. To this end, various process design and operating conditions were investigated such as multi-bed configurations, cycle parameters

and pressure/vacuum swing operation. Adsorption beds are designed to process a 95:5 mol% oxygen-argon, 68 t d^{-1} raffinate stream of a new-generation containerised O_2 VSA plant recently commercialized by Linde [32]. The adsorbent selected for the present study is Bergbau-Forschung carbon molecular sieve (B-F CMS), which has been successful in its application to pressure swing adsorption for air separation [33,34]. The CMS has also shown a promising kinetic selectivity of oxygen over argon with a diffusivity ratio of around 31 [27,30]. In addition, all the physical properties, equilibrium and kinetic parameters for this adsorbent have been extensively reported in literature [27,33,35]. Another contribution of the current investigation is to assess for the first time the specific energy consumption of the integrated VSA unit for argon concentration and to evaluate its feasibility against a conventional stand-alone cryogenic distillation system.

2. PSA Mathematical Model

The adsorption dynamics of a PSA system are described by a mathematical model which couples mass, energy and momentum balances over a packed bed with appropriate boundary conditions for each cycle step [36].

Assuming that the gas flow is governed by an axially dispersed plug flow model, the component mass balance is given by:

$$\frac{\partial c_i}{\partial t}+\frac{\partial J_i}{\partial z}+\frac{\partial\left(u\cdot c_i\right)}{\partial z}+\frac{1-\varepsilon}{\varepsilon}\cdot\rho_s\cdot\frac{\partial\overline{q}_i}{\partial t}=0 \tag{1}$$

where $J_i=-D_z\cdot c_T\cdot\frac{\partial y_i}{\partial z}$ (2)

Along with the component mass balance, an overall mass balance needs to be solved for estimating the gas velocity along the column:

$$\frac{\partial c_T}{\partial t}+\frac{\partial(u\cdot c_T)}{\partial z}+\frac{1-\varepsilon}{\varepsilon}\cdot\rho_s\cdot\sum_{i=1}^{n}\frac{\partial\overline{q}_i}{\partial t}=0 \tag{3}$$

As the column undergoes temperature variations caused by the heat of adsorption, the energy balance is represented by:

$$\frac{\partial U_g}{\partial t}+\frac{1-\varepsilon}{\varepsilon}\cdot\frac{\partial U_s}{\partial t}+\frac{\partial J_T}{\partial z}+\frac{\partial\left(u\cdot H_g\right)}{\partial z}-\frac{1-\varepsilon}{\varepsilon}\cdot\rho_s\cdot\sum_{i=1}^{n}(-\Delta H_i)\cdot\frac{\partial\overline{q}_i}{\partial t}+\frac{4\cdot h_w}{D_c}\left(T-T_w\right)=0 \tag{4}$$

where $J_T=-k_z\cdot\frac{\partial T}{\partial z}$ (5)

As the PSA and VSA cycles investigated in this study are not rapid, the effect of the kinetic energy on adsorption dynamics was neglected [37], whereas T_w in Eq.(4) was assumed to be equal to ambient temperature (303.15 K) since a heat balance around the wall was deemed negligible.

To evaluate the pressure drops along the column length, the Ergun equation [38] was taken as a momentum balance:

$$-\frac{dP}{dz}=\frac{150\cdot\mu\cdot(1-\varepsilon)^2\cdot u}{d_P^2\cdot\varepsilon^2}+\frac{1.75\cdot(1-\varepsilon)\cdot\rho_g\cdot u\cdot|u|}{d_P\cdot\varepsilon} \tag{6}$$

The boundary conditions for the gas phase concentrations and the enthalpies are given by the Danckwerts boundary conditions. With the convention that the flow direction from 0 (feed end) to L (product end) is positive, these can be written in a general form as:

$$J_i\big|_{z=0}=\frac{u+|u|}{2}\cdot\left(c_{i,0-}-c_{i,0}\right) \tag{7}$$

$$J_i\big|_{z=L_c}=\frac{u-|u|}{2}\cdot\left(c_{i,L_c+}-c_{i,L_c}\right) \tag{8}$$

$$J_T\big|_{z=0}=\frac{u+|u|}{2}\cdot\left(H_{g,0-}-H_{g,0}\right) \tag{9}$$

$$J_T\big|_{z=L_c}=\frac{u-|u|}{2}\cdot\left(H_{g,L_c+}-H_{g,L_c}\right) \tag{10}$$

Experimental adsorption equilibrium of oxygen and argon on B-F CMS were reported in the literature [27] at 303 K in the pressure range of 0–13 bar, which fully covers the range of operating pressures of the (V)PSA systems investigated in this study. Multicomponent adsorption equilibria were predicted by the ideal adsorbed solution theory (IAST), whose formulation consists in the solution of the following system of algebraic-integral equations [39,40]:

$$P\cdot y_i=P_i^0\cdot x_i \tag{11}$$

$$\psi_i=\int_0^{P_i^0}q_i\cdot d\left(\ln P_i\right) \tag{12}$$

$$\psi_i=\psi_{eq} \tag{13}$$

$$\frac{1}{q_T}=\sum_{i=1}^{n}\left(\frac{x_i}{q_i}\right) \tag{14}$$

In accordance with the fitting provided by Ma et al. [27], the pure component adsorption isotherms were described by the Langmuir model:

$$q_i^*=\frac{q_{s,i}\cdot b_i\cdot P_i}{1+b_i\cdot P_i} \tag{15}$$

where $b_i=b_{i,0}\cdot\exp\left(\frac{-\Delta H_i}{R\cdot T}\right)$ (16)

It has been extensively reported in the literature that micropore diffusion is the controlling mechanism in the adsorption of oxygen and argon on B-F CMS adsorbent [33,41,42]. In this work the micropore diffusivities were assumed to be concentration-

dependent based on the gradient of chemical potential as the true driving force for diffusion [43,44]. In addition, it was assumed that the micropore diffusivities were temperature-independent as the maximum temperature swing in the (V)PSA cycles was only 5°C. The resulting mass transfer rate was described by the following micropore diffusion model that is valid for a binary Langmuir system:

$$\frac{\partial q_i}{\partial t} = \frac{1}{r^2} \cdot \left[\frac{\partial}{\partial r} \left(D_i \cdot r^2 \cdot \frac{\partial q_i}{\partial r} \right) \right] \tag{17}$$

$$\frac{\partial \overline{q_i}}{\partial t} = \frac{3}{r_c} \cdot D_i \cdot \left. \frac{\partial q_i}{\partial r} \right|_{r=r_c} \tag{18}$$

$$D_i = \frac{D_{i,0}}{1-\theta_i-\theta_j} \cdot \left[\left(1-\theta_j\right) + \theta_i \cdot \frac{\partial q_j / \partial r}{\partial q_i / \partial r} \right] \tag{19}$$

with the following boundary conditions:

$$q_i\big|_{r=r_c} = q_i^* \tag{20}$$

$$\left. \frac{\partial q_i}{\partial r} \right|_{r=0} = 0 \tag{21}$$

Values for the limiting diffusivity time constants ($D_{i,0}/r_c^2$) of oxygen and argon on B-F CMS adsorbent were also obtained from the work by Ma et al. [27]. A complete list of physical properties, equilibrium and kinetic parameters for the CMS considered in this study along with the relevant references can be found in Table 1.

Table 1. Physical properties, equilibrium and kinetic parameters for CMS adsorbent

Property / Parameter	***Value***	***Reference***
Manufacturer	Bergbau-Forschung	
ρ_s (kg m^{-3})	987.7	[33]
d_p (m)	3.175 x 10^{-3}	
$c_{p,s}$ (J kg^{-1} K^{-1})	1,046	[35]
$q_{s,Ar}$ / $q_{s,O2}$ (mol kg^{-1})	1.62 / 1.62	Regressed from [27]
b_{Ar} / b_{O2} (bar^{-1}) @303 K	0.197 / 0.262	
$b_{0,Ar}$ / $b_{0,O2}$ (bar^{-1})	3.44 x 10^{-4} / 4.77 x 10^{-4}	Calculated
ΔH_{Ar} / ΔH_{O2} (kJ mol^{-1})	16.0 / 15.9	Ar: [45] O_2: [35]
$(D_0/r_c^2)_{Ar}$ / $(D_0/r_c^2)_{O2}$ (s^{-1}) @303 K	1.7 x 10^{-4} / 5.2 x 10^{-3}	[27]

The values of transport properties were calculated employing typical correlations for packed beds. Axial mass dispersion coefficient D_z and axial thermal dispersion coefficient k_z were estimated using the correlations by Wakao and Funazkri [46]:

$$\frac{\varepsilon \cdot D_z}{D_m} = 20 + 0.5 \cdot Sc \cdot Re$$

(22)

$$\frac{k_z}{k_g} = 7 + 0.5 \cdot Pr \cdot Re \quad (23)$$

The internal heat transfer coefficient between the gas and the column wall was calculated with the correlation by Specchia et al. [47]:

$$h_w = \frac{k_g}{d_P} \cdot \left(0.0835 \cdot Re^{0.91}\right) \quad (24)$$

Physical properties of the gas mixture including density, thermal conductivity, viscosity and molar specific heat were evaluated using Multiflash embedded within gPROMS software [48] and considering the ideal gas law. As a result, each physical property that is a function of pressure, temperature and composition varied in both temporal and spatial domains in the simulations.

Besides, adsorption beds need to be coupled with ancillary equipment in order to simulate a realistic flowsheet [49]. The modelling of these ancillary units was carried out as follows:

- Valves: they were modelled to operate as a mass flow controller (MFC) or in pressure-driven mode (PDM):

  $F = F_i$ (MFC) (25)

  $F = V_{SP} \cdot C_v \cdot \sqrt{\Delta P}$ (PDM) (26)

  where C_v is the valve flow coefficient and V_{SP} is the valve stem position ranging 0–1. Stream information, such as pressure, temperature and gas composition, are passed through the valve to the neighbouring units.
- Headers: they were modelled as perfectly-mixed continuous stirred tank reactors (CSTRs) allowing an arbitrary number of connections. The volume of each header was assumed 1% of the internal column volume.
- Sources/Sinks: they were modelled as boundary conditions of the whole PSA system, e.g. feed streams flowing into the PSA and product streams leaving the PSA.

Since argon diffuses more slowly than oxygen in B-F CMS [27,30,33] it is concentrated in the raffinate stream during the adsorption step while oxygen is extracted in the offgas stream during blowdown and self-purge steps. The key performance indicators of a (V)PSA cycle for this separation are argon purity, argon recovery, bed productivity and specific energy consumption. They are calculated by the following equations:

$$Ar\ Purity = \frac{\int_0^{t_{AD}} c_{Ar} \cdot u\big|_{z=L_c}\, dt}{\sum_{i=1}^{n} \int_0^{t_{AD}} c_i \cdot u\big|_{z=L_c}\, dt} \tag{27}$$

$$Ar\ Recovery = \frac{\int_0^{t_{AD}} c_{Ar} \cdot u\big|_{z=L_c}\, dt}{\int_0^{t_{AD}} c_{Ar} \cdot u\big|_{z=0}\, dt + \int_0^{t_{FP}} c_{Ar} \cdot u\big|_{z=0}\, dt} \tag{28}$$

$$Bed\ Productivity = \frac{\left(\int_0^{t_{AD}} c_{Ar} \cdot u\big|_{z=L_c}\, dt\right) \cdot A_c}{t_{cycle} \cdot m_{ads}} \tag{29}$$

$$Specific\ Energy = \frac{\int_0^{t_{AD}+t_{FP}} Power_{compressor} dt + \int_0^{t_{BD}+t_{SP}} Power_{vacuum} dt}{\left(\int_0^{t_{AD}} c_{Ar} \cdot u\big|_{z=L_c}\, dt\right) \cdot MW_{Ar} \cdot A_c} \tag{30}$$

$$Power_{compressor} = \frac{1}{\eta_c} \cdot F \cdot \frac{\gamma}{\gamma - 1} \cdot \left(\frac{P_{atm}}{\rho_g}\right) \cdot \left[\left(\frac{P_{ads}}{P_{atm}}\right)^{\frac{\gamma-1}{\gamma}} - 1\right] \tag{31}$$

$$Power_{vacuum} = \frac{1}{\eta_v} \cdot F \cdot \frac{\gamma}{\gamma - 1} \cdot \left(\frac{P_{des}}{\rho_g}\right) \cdot \left[\left(\frac{P_{atm}}{P_{des}}\right)^{\frac{\gamma-1}{\gamma}} - 1\right] \tag{32}$$

where Eqs. (30–32) relate to calculation of the specific energy required for the separation. This specific energy consumption is calculated directly by dividing the sum of the power consumption in running either the compressor in the PSA cycles or the compressor and the vacuum pump in the VSA cycles by the amount of argon produced after its cyclic steady state (CSS) is achieved. For all the (V)PSA configurations of this study the cyclic steady states were reached after around 40–50 cycles with differences of Ar purity and recovery between the new and previous cycles both less than 10^{-5} .

In all simulations the differential-algebraic equations (DAEs) were solved using gPROMS software [48]. Spatial domains were discretized by the second order centered finite difference method (CFDM) with 100 elements in the axial domain along the column and 20 elements in the radial domain in the micropore. The absolute and relative numerical tolerances were both set to 10^{-6}.

3. Simulation Basis and Cycle Configuration

The aim of this work is to design an industrial Ar concentration (V)PSA unit processing a 95:5 mol% oxygen-argon mixture with a flowrate of 68 t d^{-1} that is approximately equivalent to 24.53 mol s^{-1} or 0.60 sm^3 s^{-1} and corresponds to the capacity of the new O_2 VSA C-series commercialized by Linde. These new-generation containerised units are characterized by

ease of operation and service as well as low energy consumption and maintenance [32]. Firstly, PSA simulations were carried out where the adsorption pressure and the desorption pressure were set at 3 bar and 1.013 bar, respectively. The pressure levels were the same as those of the Lindox process, the commercialised PSA system designed for air separation [31,34]. However, it turned out that the performance of the PSA system was unsatisfactory in that the argon purity was around 22% at best under the conditions of an argon recovery being higher than 50%. Instead of PSA, various VSA processes with the operational pressure range of 0.1–1 bar were trialled for enhancing the performance [30,34]. It has been reported that the argon purity can be improved substantially by having a VSA cycle rather than a PSA cycle with the argon recovery maintained as high as those of PSA, but the gain of argon purity is achievable only with a high mechanical energy consumption required for the evacuation step [50].

In both PSA and VSA simulations the column diameter was determined to have a superficial velocity in the vicinity of 0.1 m s^{-1} that is typical of industrial (V)PSA units, while the L/D ratio was selected in order to obtain a total cycle time of 2–4 min and a maximum pressure drop along the bed of 0.03 bar. The resulting column geometry along with the calculated transport properties and the operating conditions are listed in Table 2 for both PSA and VSA systems. It should be noted that the transport properties differ between the PSA and VSA systems because the operating pressures are different. The correlations are in fact function of the Reynolds number that contains pressure.

Table 2. Column parameters and operating conditions of PSA and VSA systems

Column parameters	***PSA***	***VSA***
L_c (m)	8.0	5.6
D_c (m)	1.6	2.8
ε (-)	0.4	
D_z (m^2 s^{-1})	7.4×10^{-4}	1.4×10^{-3}
K_z (W m^{-1} K^{-1})	0.73	0.37
h_w (W m^{-2} K^{-1})	28.4	10.4
Operating conditions	***PSA***	***VSA***
Feed composition (mol%)	5% Ar ; 95% O_2	
Adsorption pressure (bar)	3	1.013
Desorption pressure (bar)	1.013	0.1
Feed temperature (K)	303.15	
Molar feed flowrate (mol s^{-1})	24.53 (or 0.60 sm^3 s^{-1})	
Volumetric feed flowrate (m^3 s^{-1})	0.20	0.61

In a kinetically-controlled separation the difference in the diffusion rates of the adsorbing gases has to be exploited so that the adsorption step must be short enough to prevent the

system from approaching equilibrium but not so short as to preclude significant uptake. A major disadvantage using a conventional Skarstrom cycle is that the slowly diffusing raffinate product would be continuously consumed during the purge step decreasing substantially the recovery [34]. This issue can be overcome by incorporating a self-purge step in the cycle in place of the conventional purge step. By simply closing the bed at the product end and leaving it for a period of time at low operating pressure, the oxygen will come off first followed by argon so that the system is self-purging. The use of the self-purging step has been extensively studied theoretically and validated experimentally in the context of kinetically-controlled pressure swing air separation [33,43]. Most modern nitrogen-production PSA units operate on a cycle which incorporates a self-purging desorption step [34]. The first cycle configuration investigated in this study was a 1-bed 4-step Skarstrom cycle with a self-purge step, as depicted in Figure 1. As a result of having no purge from another bed it is possible to operate the cycle with only one bed.

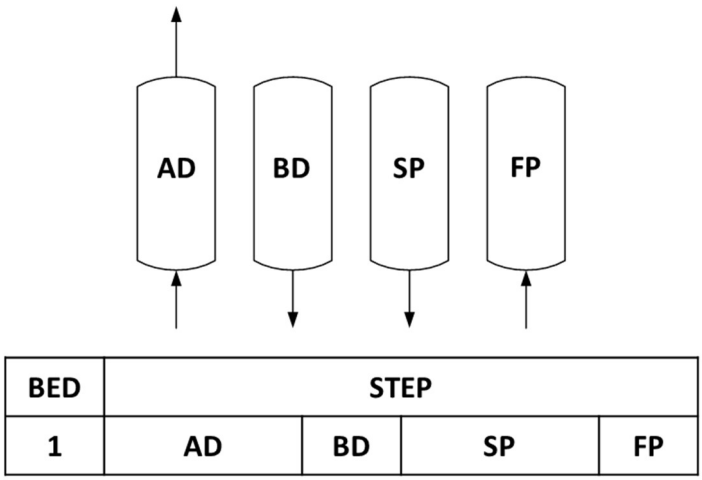

Figure 1. Configuration of a 1-bed 4-step cycle (AD: Adsorption, BD: Blowdown, SP: Self-purge, FP: Feed pressurization; $t_{AD} = t_{SP}$, $t_{BD} = t_{FP}$)

It is well known that the incorporation of a pressure equalization step in a PSA cycle improves the separation performance by increasing, for instance, the raffinate recovery at the same raffinate purity. The pressure equalization step conserves energy because the compressed gas from a high-pressure bed is used to partially pressurize a low-pressure bed [34]. In particular, Hassan et al. [33] have proposed a kinetically-controlled PSA air separation process with a double-ended pressure equalization in which the feed and product ends of the high-pressure bed and low-pressure bed are connected. It was claimed that this modification enables quicker pressure equalization and improves the raffinate recovery [33]. Following the latter reference the second configuration analysed in this work was a 2-bed 6-step cycle with schematic outlined in Figure 2.

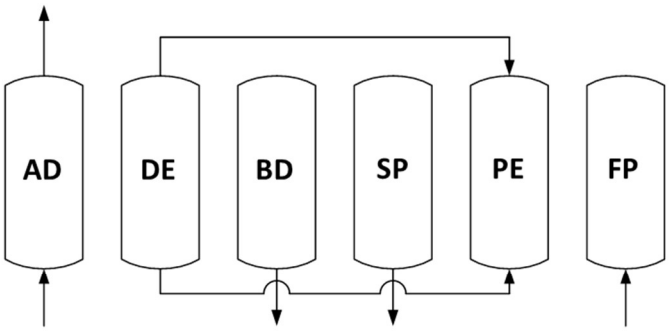

BED	STEP					
1	AD	DE	BD	SP	PE	FP
2	SP	PE	FP	AD	DE	BD

Figure 2. Configuration of a 2-bed 6-step cycle (AD: Adsorption, DE: Depressurizing pressure equalization, BD: Blowdown, SP: Self-purge, PE: Pressurizing pressure equalization, FP: Feed pressurization; $t_{AD} = t_{SP}$, $t_{BD} = t_{FP}$, $t_{DE} = t_{PE}$)

To further improve the PSA unit performance a novel 3-bed 9-step cycle configuration was also devised. Compared to the 2-bed 6-step cycle, the number of column had to increase by one in order to incorporate the second pressure equalization step into the cycle. The new cycle was constructed in reference to a 3-bed configuration found in a patent [51] and it was tailored to include the steps required for kinetic separation discussed above. In accordance with the graphical approach for complex PSA cycle scheduling developed by Ebner et al. [52], the resulting cycle configuration was equipped with two double-ended pressure equalization steps, a self-purge step, and an idle step placed in between the two depressurizing pressure equalization steps, as shown in Figure 3. Note that the idle step is required for bed synchronization purposes and that in a multi-bed PSA system involving three or more beds each step duration is a fixed fraction of the total cycle time.

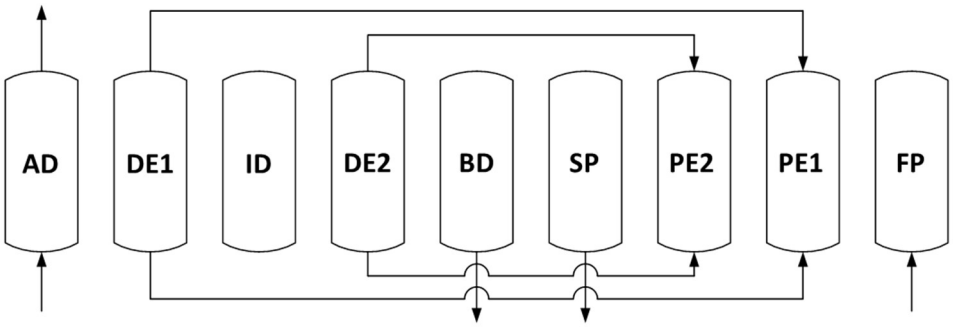

BED	STEP									
1	AD		DE1	ID		DE2	BD	SP	PE2	PE1	FP
2	SP	PE2	PE1	FP	AD		DE1	ID	DE2	BD	SP
3	ID	DE2	BD	SP		PE2	PE1	FP	AD	DE1	ID

Figure 3. Configuration of a 3-bed 9-step cycle (AD: Adsorption, DE: Depressurizing pressure equalization, ID: Idle, BD: Blowdown, SP: Self-purge, PE: Pressurizing pressure equalization, FP: Feed pressurization; $t_{AD} = t_{SP} = t_{ID} = t_{CYCLE}/6$, $t_{BD} = t_{FP} = t_{DE1} = t_{PE1} = t_{DE2} = t_{PE2} = t_{CYCLE}/12$)

As the most crucial element in a kinetic separation PSA is represented by the adsorption and desorption step time it has been explored in detail the effect of this cycle parameter on both PSA and VSA performances. Table 3 reports the information on cycle step times for the 1-bed, 2-bed and 3-bed cycle configurations investigated in this study.

Table 3. Cycle step times for the 1-bed, 2-bed and 3-bed configurations for PSA and VSA

1-bed 4-step configuration	
$t_{AD} = t_{SP}$ (s)	40 / 50 / 60 / 70
$t_{BD} = t_{FP}$ (s)	30
t_{CYCLE} (s)	140 / 160 / 180 / 200
2-bed 6-step configuration	
$t_{AD} = t_{SP}$ (s)	30 / 40 / 50 / 60
$t_{BD} = t_{FP}$ (s)	30
$t_{DE} = t_{PE}$ (s)	5
t_{CYCLE} (s)	130 / 150 / 170 / 190
3-bed 9-step configuration	
$t_{AD} = t_{SP} = t_{ID}$ (s)	25 / 30 / 35 / 40
$t_{BD} = t_{FP} = t_{DE1} = t_{PE1} = t_{DE2} = t_{PE2}$ (s)	12.5 / 15 / 17.5 / 20
t_{CYCLE} (s)	150 / 180 / 210 / 240

In all simulations it was assumed that the columns were initially filled with pure argon at the proper adsorption, desorption or intermediate pressures depending on the PSA cycle schedule and at the temperature of 303.15 K. According to the operational pressure swing range of the simulations valve flow coefficients were calibrated with reference to the cycle

step(s) in which the valves were open, with their values summarized in Table 4. Figure 4 provides a schematic of one adsorption bed with the column ancillary equipment and shows the location of the valves listed in Table 4.

Table 4. Valve flow coefficients of PSA and VSA systems

Valve	***C_v (kg s^{-1} $Pa^{-1/2}$)***	
	PSA	***VSA***
Feed (V_F)	1.0×10^{-3}	1.0×10^{-3}
Product (V_P)	1.0×10^{-3}	1.0×10^{-3}
Blowdown (V_{BD})	5.0×10^{-4}	1.5×10^{-3}
Self-purge (V_{SP})	5.0×10^{-4}	1.5×10^{-3}
Equalization top (V_{ET})	1.0×10^{-4}	3.0×10^{-4}
Equalization bottom (V_{EB})	1.0×10^{-4}	3.0×10^{-4}

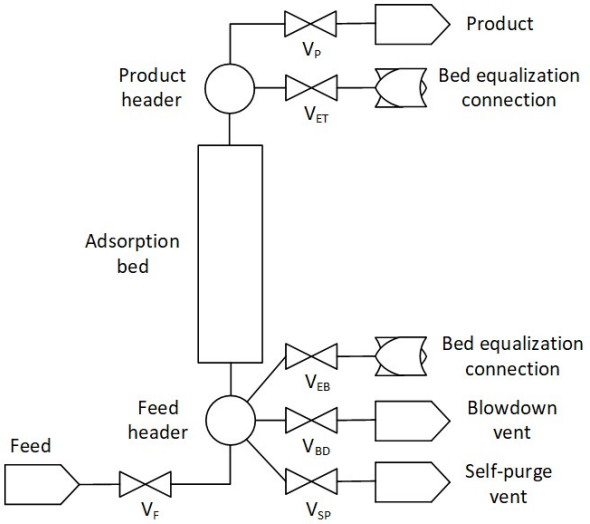

Figure 4. Schematic of (V)PSA system represented by one adsorption bed with ancillary equipment

4. Results and Discussion

4.1 PSA Simulations

As mentioned earlier it was anticipated that a single-stage PSA would not be sufficient to produce argon with a purity of 98+%. To enhance the purity of argon product, a two-stage PSA system was devised in this study. The first-stage PSA was designed as an Ar enriching step aiming to increase substantially the Ar purity with the Ar recovery maintained at least 50%. The following second-stage PSA was regarded as an Ar purification step for boosting the Ar purity up to the target with the sacrifice of the Ar recovery. A total of twelve simulation runs were carried out for the first-stage PSA process involving the 1-bed, 2-bed and 3-bed cycle configurations discussed in the previous section. For each configuration it was assessed how the adsorption step time affected the unit performance in terms of Ar purity, Ar recovery, bed productivity and specific energy consumption, calculated by Eqs. (27–31). In calculating the

energy consumption a compressor efficiency (η_c) of 80% was considered, which in line with industrial compressors used in air separation plants [11,13]. The feed was compressed from atmospheric pressure to 3.1 bar in order to overcome the pressure drop across the mass flow controller and the adsorption bed. As a result of the numerical simulation campaign, the PSA operating parameters and the associated performance results at cyclic steady state are given in Table 5. The unit KPIs are also depicted in Figure 5 as a function of the adsorption step time.

Table 5. Performance results of the PSA systems

Run #	***P_{ads} (bar)***	***P_{des} (bar)***	***t_{AD} (s)***	***Ar purity (%)***	***Ar recovery (%)***	***Bed productivity ($mol_{Ar}\ h^{-1}\ kg_{ads}^{-1}$)***	***Specific energy consumption ($MJ\ kg_{Ar}^{-1}$)***	***O_2 purity in offgas (%)***	***O_2 recovery in offgas (%)***
1-bed PSA									
Run 1	3	1.013	40	19.1	49.0	0.065	4.24	97.1	89.1
Run 2			50	16.1	54.0	0.078	3.85	97.2	85.2
Run 3			60	14.2	57.9	0.089	3.59	97.4	81.6
Run 4			70	12.7	61.1	0.099	3.40	97.5	77.9
2-bed PSA									
Run 5	3	1.013	30	20.1	53.8	0.057	3.86	97.3	88.7
Run 6			40	16.3	59.3	0.073	3.50	97.5	84.0
Run 7			50	13.8	63.5	0.086	3.27	97.6	79.1
Run 8			60	12.2	66.7	0.098	3.11	97.7	74.7
3-bed PSA									
Run 9	3	1.013	25	22.2	50.0	0.039	4.15	97.2	90.8
Run 10			30	16.9	58.3	0.045	3.56	97.5	84.9
Run 11			35	13.4	64.3	0.050	3.23	97.7	78.1
Run 12			40	11.4	68.3	0.053	3.04	97.8	72.1

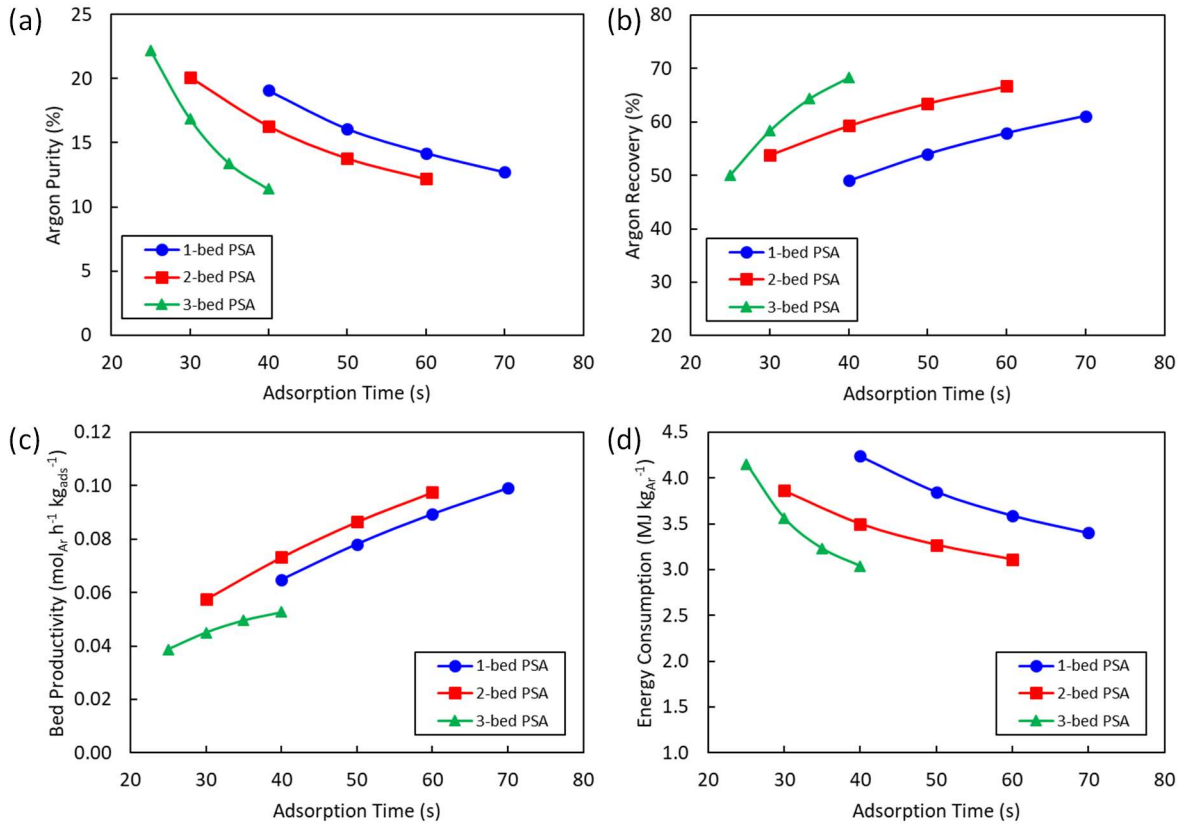

Figure 5. Evolution of the PSA unit KPIs with the adsorption step time: (a) Argon purity; (b) Argon recovery; (c) Bed productivity; (d) Specific energy consumption. PSA operating parameters are reported in Table 5

As expected, the PSA performance is significantly affected by the adsorption step time and there is always a trade-off between argon purity and recovery while both bed productivity and specific energy consumption change favourably with increasing adsorption time (Figure 5). For each configuration, longer adsorption times improve argon recovery because more argon is withdrawn from the column during the prolonged high-pressure adsorption step but argon purity decreases as more oxygen travels to the product end contaminating the raffinate product. Similarly, bed productivity increases with the adsorption step time following the trend of recovery while the specific energy consumption reduces as more argon is collected in the raffinate product. Compared to the 1-bed PSA simulation runs the 2-bed PSA configuration exhibited argon recovery increasing by around 5% on average at the same argon purity, due to the incorporation of the pressure equalization step. For instance, both Run 2 of the 1-bed PSA and Run 6 of the 2-bed PSA achieved an argon purity slightly higher than 16%, but Run 6 showed an argon recovery of 59.3% in comparison to 54.0% of Run 2. The effect of the second pressure equalization step of the 3-bed PSA configuration was so marginal that the 3-bed PSA could achieve 59.6% of argon recovery at the same argon purity, only 0.3% increase from that of the 2-bed PSA. Note that the argon recovery of the 3-bed PSA was estimated by data interpolation of Runs 10 and 11. This can be explained by the combination

of multiple pressure equalization steps but a shorter blowdown step compared to the total cycle time. This was dictated by the cycle configuration and led to an incomplete bed regeneration, even with a shorter adsorption step time. It is expected that a PSA running with a greater extent of pressure swing between adsorption and desorption would benefit from having more pressure equalization steps in place. The 3-bed configuration showed the lowest bed productivity (Figure 5c) as a result of the lowest ratio of adsorption step time over total cycle time. It is worth noticing that Table 5 also reports the oxygen purity and recovery obtained in the offgas. All the simulations showed that the proposed PSA system could purify the oxygen further to 97+% with good recoveries, enabling to use the purified oxygen for some industrial applications such as fuel cell technology [53].

Figures 6–8 show the pressure and temperature profiles averaged over the column during a cycle at the cyclic steady state for Runs 2, 7 and 10, respectively. In the 2-bed configuration the bed pressure equalizes at 1.86 bar (Figure 7a) while in the 3-bed configuration the two equalizations occur at 2.14 bar and 1.62 bar (Figure 8a). It is worth noticing that the maximum temperature swing over a cycle was around 5°C for all the configurations, which is rather close to the results presented by Jee et al. [54] where they also studied a PSA for oxygen purification having the same feed.

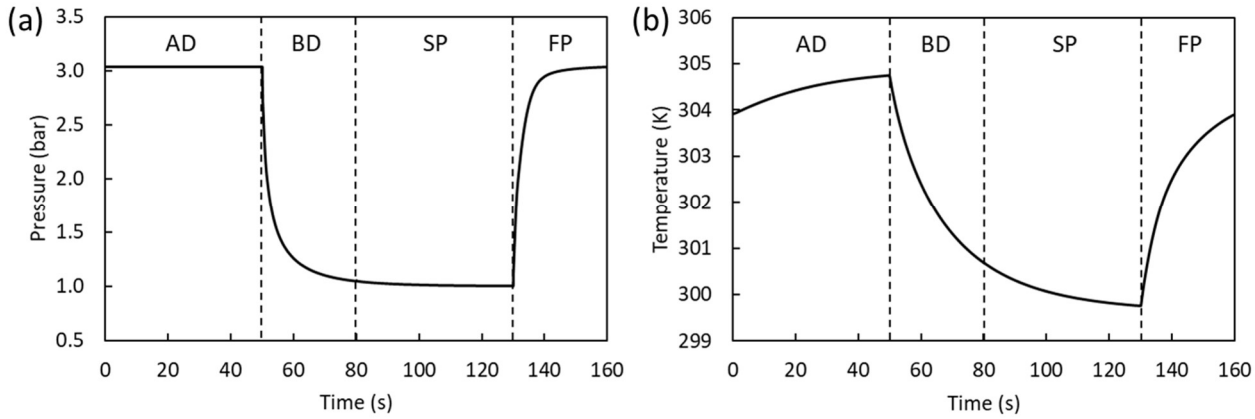

Figure 6. Profiles of (a) pressure and (b) temperature averaged over the column for a cycle at the cyclic steady state of the 1-bed 4-step PSA system (Run 2)

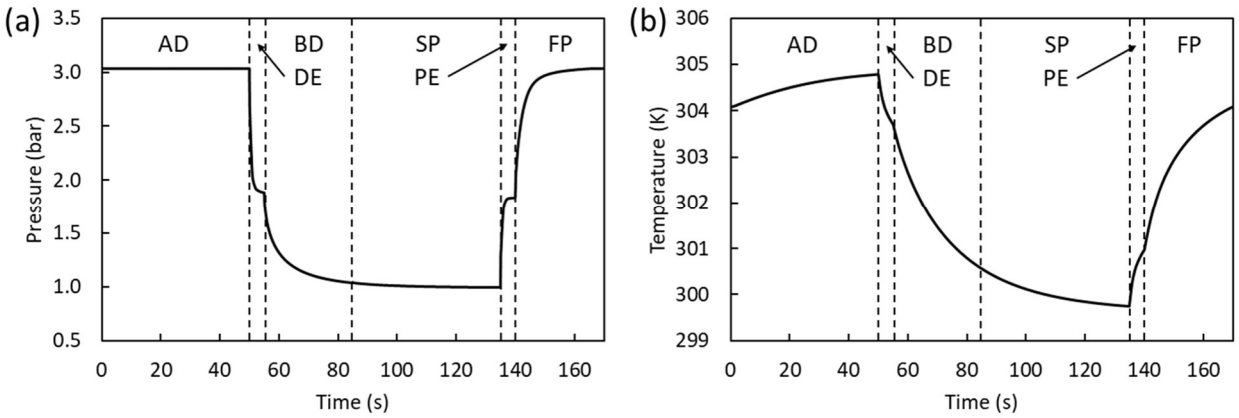

Figure 7. Profiles of (a) pressure and (b) temperature averaged over the column for a cycle at the cyclic steady state of the 2-bed 6-step PSA system (Run 7)

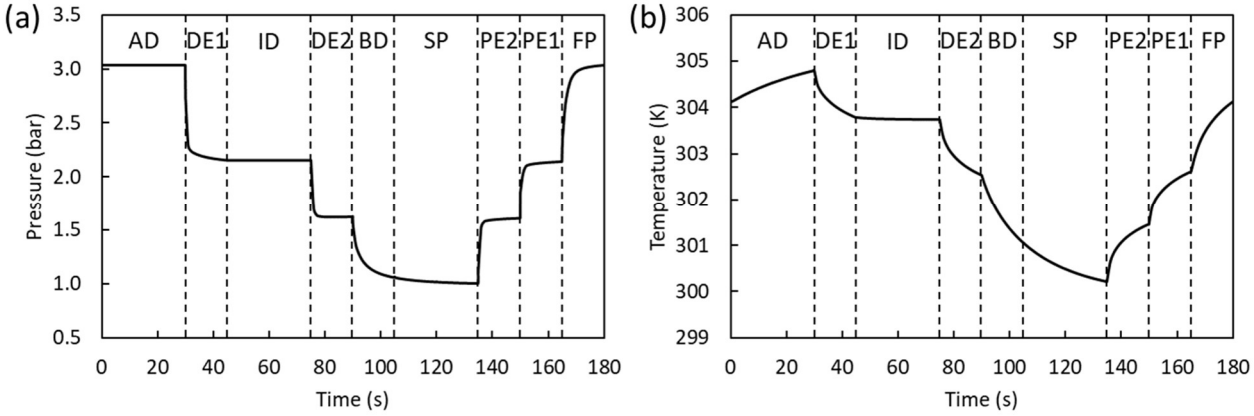

Figure 8. Profiles of (a) pressure and (b) temperature averaged over the column for a cycle at the cyclic steady state of the 3-bed 9-step PSA system (Run 10)

4.2 VSA Simulations

The maximum argon purity achievable in the single-stage PSA process was 22.2% with a recovery of 50.0%. This purity, obtained with a 3-bed configuration (Run 9), was deemed too low for the argon product specification, even considering a potential second-stage PSA. On the other hand, the argon purity of the first-stage unit may be improved by taking VSA rather than PSA. For this reason another set of twelve simulation runs were carried out considering an atmospheric adsorption pressure and a vacuum desorption pressure. Similarly to the PSA units, a compressor was installed to boost the feed pressure of the VSA units from atmospheric pressure to 1.1 bar in order to overcome the pressure drop across the mass flow controller and the adsorption bed. Given the volumetric feed flowrate of 0.61 $m^3\ s^{-1}$ it has been reported that industrial liquid ring vacuum pumps can be designed to achieve low suction pressures below 0.1 bar, as exemplified by the LR Series commercialized by Edwards [55]. Consulting the vendor's performance data the vacuum pump efficiency (η_v) was evaluated at 40% for a suction pressure of 0.1 bar, which is comparable with the experimental

results reported by Krishnamurthy et al. [56]. VSA simulations were carried out for the 1-bed and 2-bed configurations only because it was found that the 3-bed configuration could not improve much the unit performance as with the PSA runs. Table 6 reports the operating parameters and the associated performance results at cyclic steady state of the VSA runs.

Table 6. Performance results of the VSA systems

Run #	*P_{ads} (bar)*	*P_{des} (bar)*	*t_{AD} (s)*	*Ar purity (%)*	*Ar recovery (%)*	*Bed productivity ($mol_{Ar}\ h^{-1}\ kg_{ads}^{-1}$)*	*Specific energy consumption ($MJ\ kg_{Ar}^{-1}$)*	*O_2 purity in offgas (%)*	*O_2 recovery in offgas (%)*
1-bed VSA									
Run 13	1.013	0.1	40	65.6	38.8	0.024	27.2	96.8	98.9
Run 14			50	51.1	47.0	0.032	22.1	97.2	97.6
Run 15			60	39.4	52.9	0.038	19.2	97.5	95.7
Run 16			70	31.5	57.3	0.043	17.3	97.7	93.4
Run 17		0.05	50	58.3	44.2	0.030	33.8	97.1	98.3
Run 18		0.2		35.8	52.4	0.035	12.4	97.4	95.1
2-bed VSA									
Run 19	1.013	0.1	30	64.1	41.6	0.021	25.3	97.0	98.8
Run 20			40	50.8	50.9	0.029	20.3	97.4	97.4
Run 21			50	39.1	57.5	0.037	17.6	97.7	95.3
Run 22			60	31.0	62.4	0.043	15.7	97.9	92.7
Run 23		0.05	40	57.6	48.2	0.028	30.9	97.3	98.1
Run 24		0.2		35.7	56.4	0.032	11.5	97.6	94.7

Apart from the adsorption step time, Runs 17, 18 and Runs 23, 24 assessed the 1-bed and 2-bed unit performance when they were operated at different vacuum desorption pressure of 0.05 and 0.2 bar. From Table 6 it is evident that with the lower desorption pressure the beds are better regenerated and have higher adsorption capacity in the subsequent adsorption step, thus improving argon purity and deteriorating argon recovery. As expected, the specific energy consumption is highly sensitive to the desorption pressure as it nearly tripled with the desorption pressure decreasing from 0.2 bar (Runs 18, 24) to 0.05 bar (Runs 17, 24). In the VSA simulation runs the use of a 2-bed configuration with the pressure equalization step exhibited around 4% greater argon recovery than the 1-bed configuration.

Overall, the VSA KPIs showed the same trends as the PSA counterparts and it should be noted that, with a recovery close to 50%, argon purity more than doubled up to 51.1% in Run 14 and 50.8% in Run 20. Changing the operation mode of PSA to VSA is one of the efficient ways for improving argon purity because the corresponding loss of argon recovery during the blowdown and self-purge steps of the VSA process is relatively low compared to that of the

PSA process. The enhanced argon purity came at the expenses of both bed productivity and specific energy consumption. The VSA beds were around 2.5 times less productive than the PSA beds mainly due to the increased adsorbent inventory in the bed. The vacuum pumps of VSA required around 6 times more specific power consumption than the compressors of PSA due to the VSA operating with an increased pressure ratio and a reduced turbomachinery efficiency. A summary of KPIs trade-offs for the VSA process is shown in Figure 9 where the adsorption step time and vacuum desorption pressure varied.

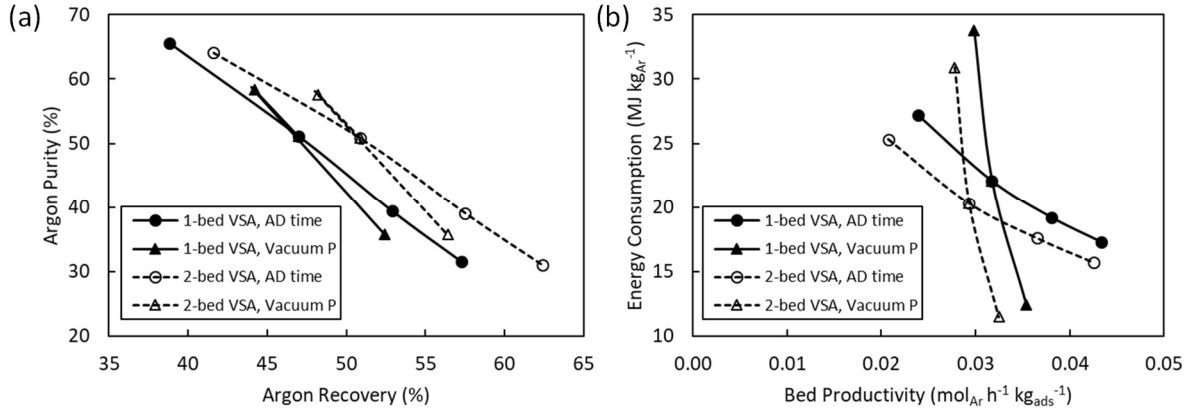

Figure 9. Key performance indicators trade-offs for the VSA process with varying adsorption step time and vacuum desorption pressure: (a) Argon purity against argon recovery and (b) Specific energy consumption against bed productivity. VSA operating parameters are reported in Table 6

From Table 6 and Figure 9 Run 20 was considered the best case, achieving the following performances: argon purity of 50.8%, argon recovery of 50.9%, bed productivity of 0.029 mol_{Ar} kg_{ads}^{-1} h^{-1} and specific energy consumption of 20.3 MJ kg_{Ar}^{-1}. Moreover, both oxygen purity and recovery in the offgas were estimated at 97.4%. With the same operational pressure swing and feed composition Jin et al. [31] obtained an argon purity of around 70% with a recovery of 50%. The better VSA performance can be explained as a result of using Takeda II CMS that has a diffusivity ratio of around 100, therefore three times higher than that of B-F CMS used in this study. However, kinetic data of Takeda II CMS are not comprehensive as they authors used empirical constants optimized from a set of experiments.

4.3 Effect of the Concentration Dependence of Diffusivity

It has been reported that the concentration dependence of micropore diffusivity has a strong effect on the steady-state performance of a kinetically-controlled PSA separation using CMS adsorbents, especially at high pressures [43]. According to the chemical potential theory as the driving force for micropore diffusion, the pure component diffusivity is an increasing function of the fractional adsorption coverage which can be expressed by the Darken correction factor [34]:

$$\frac{D}{D_0} = \frac{d\ln P}{d\ln q} = \frac{1}{1-\theta} = 1 + b \cdot P \tag{33}$$

The previous equation is expanded for a Langmuir isotherm for which the concentration dependence becomes very strong in the saturation region. Figure 10a shows the adsorption isotherms for oxygen and argon on B-F CMS in the pressure range investigated in this study. It is clear that, particularly for the PSA cycles, the adsorption isotherms are no longer in the linear range resulting in a Darken correction factor diverging from the unity (Figure 10b).

To assess the impact of the concentration dependence of diffusivity on argon purity and recovery at CSS, two simulation runs, namely Run 2 and Run 14 as exemplary of PSA and VSA cycles respectively, were repeated considering a constant diffusivity. The results of this sensitivity analysis on the two diffusivity models are detailed in Table 7. For the PSA system argon KPIs deviated in the range of 1.3–4.1% while, as expected, the deviations were visibly reduced to 0.7–1.5% for the VSA system. The qualitative trend of deviations between the two diffusivity models is also confirmed by works investigating the kinetically-controlled N_2 PSA process [43,57]. However, Farooq and Ruthven [43] reported higher deviations in the N_2 KPI_S, of up to 5–10% on average, with an adsorption pressure of 3 atm.

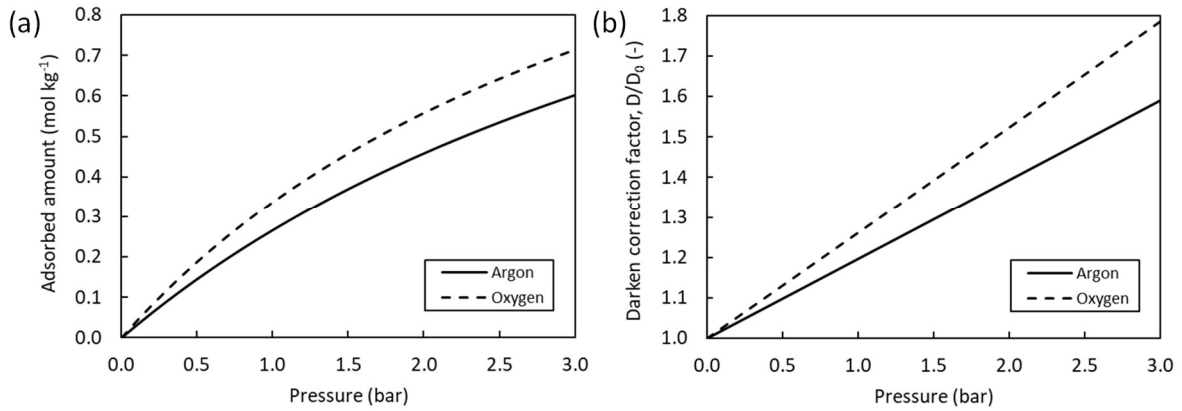

Figure 10. (a) Adsorption isotherms and (b) Darken correction factor for oxygen and argon on B-F CMS at 303.15 K. Equilibrium parameters are reported in Table 1

Table 7. Effect of constant and variable micropore diffusivity on argon purity and recovery for PSA and VSA systems

1-bed PSA						
Run #	***P_{ads} (bar)***	***P_{des} (bar)***	***t_{AD} (s)***	***Diffusivity model***	***Ar purity (%)***	***Ar recovery (%)***
Run 2	3	1.013	50	Constant D	14.8	58.1
				Variable D	16.1	54.0
1-bed VSA						
Run #	***P_{ads} (bar)***	***P_{des} (bar)***	***t_{AD} (s)***	***Diffusivity model***	***Ar purity (%)***	***Ar recovery (%)***
Run 14	1.013	0.1	50	Constant D	50.4	48.5
				Variable D	51.1	47.0

4.4 Adsorption Dynamics of PSA and VSA Processes

Figure 11 shows the profiles of both Ar and O_2 gas phase mole fraction and average adsorbed phase concentration along the dimensionless axial distance of the column at the end of adsorption step for various PSA and VSA cycles. In particular Runs 2, 6 and 10 were the simulations of the 1-bed, 2-bed and 3-bed PSA cycle configurations, respectively, with an argon purity ranging 16-17%, while Runs 14 and 20 were the 1-bed and 2-bed VSA cycle configurations with an argon purity of around 51%. In Figure 11a the VSA runs clearly exhibit sharper Ar mole fraction mass transfer zones (MTZ) than the PSA runs. Figure 11b shows that the Ar average adsorbed amounts have different starting values at the feed end for the PSA and VSA runs because of the different adsorption pressure employed in the cycles. From the figure it is expected that the greater the Ar adsorption amount near the product end gets, the lower the Ar recovery becomes. This is because more argon is likely to be lost in the blowdown and self-purge steps. As a result of these effects, the runs are listed in the order of increasing Ar recovery as follows: Run 14 (47.0%) < Run 20 (50.9%) < Run 2 (54.0%) < Run 10 (58.3%) < Run 6 (59.3%).

Similarly, the VSA process shows an O_2 mole fraction MTZ sharper than the PSA process (Figure 11c), thus anticipating higher O_2 recoveries in the offgas as oxygen is less likely to be lost during the adsorption step. Overall, comparing Figures 11c and 11d, the O_2 average adsorbed phase MTZ shows a broader shape than the O_2 gas phase MTZ, which is in accordance with what observed by Kim et al. [21] considering a similar feed composition adsorbed on Takeda CMS.

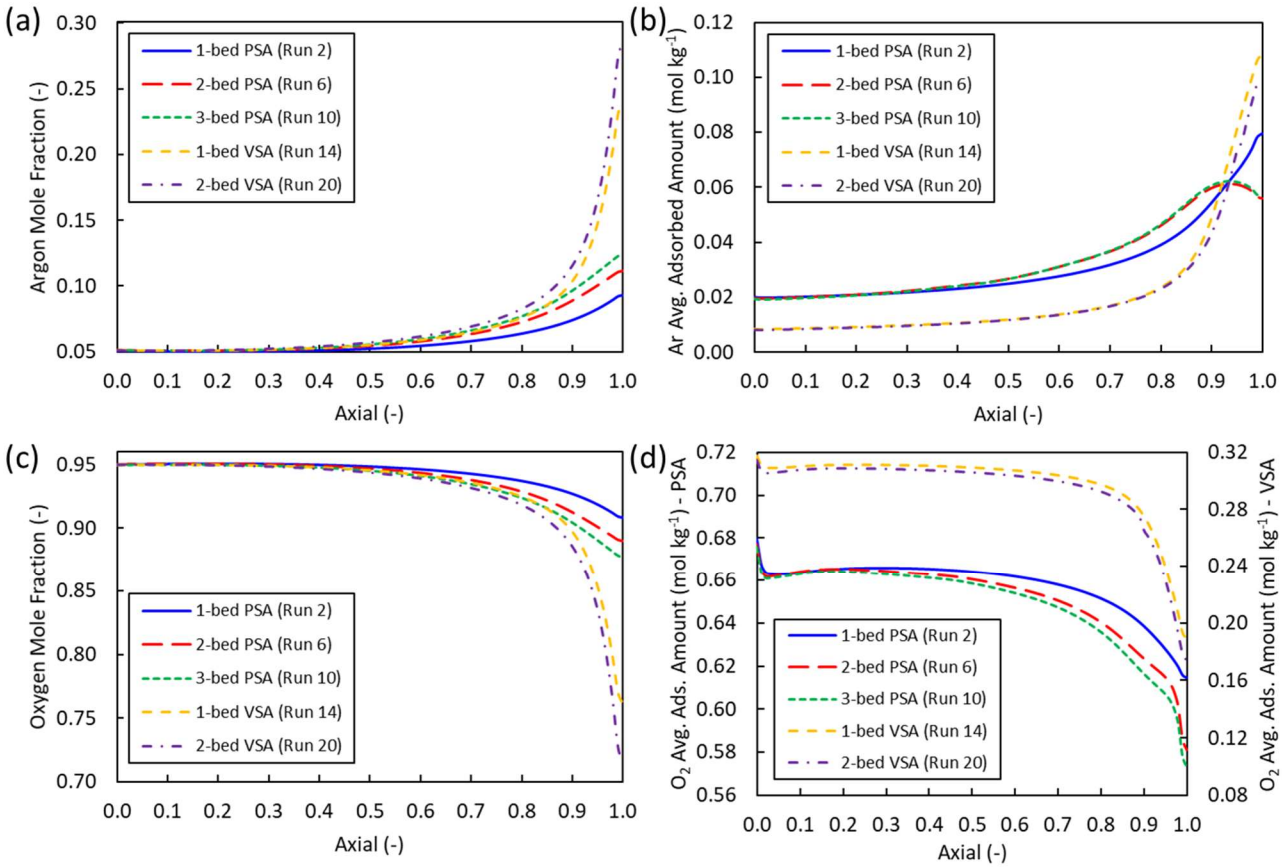

Figure 11. Profiles of (a) Ar gas phase mole fraction, (b) Ar average adsorbed phase concentration, (c) O_2 gas phase mole fraction, (d) O_2 average adsorbed phase concentration along the dimensionless axial column distance at the end of adsorption step for various PSA and VSA cycles. Simulation run information is reported in Tables 5 and 6

Adsorption dynamics of the 2-bed VSA simulation to be used as a first-stage Ar concentrator (Run 20) can be further discussed with respect to Ar and O_2 adsorbed phase concentration along the dimensionless axial column distance and radial micropore distance at the end of adsorption step. The resulting surfaces of adsorbed amount are shown in Figure 12. Comparing this figure with the corresponding curves of Run 20 in Figures 11b and 11d it is clear how the component average adsorbed amounts were averaged along the radial coordinate. For instance, at product end (Axial = 1) the O_2 average adsorbed amount in Figure 11d reports a value of around 0.18 mol kg^{-1} which is reached by the O_2 adsorbed amount in Figure 12 considering a section at Radial ≈ 0.8. For both components the largest MTZ along the radial micropore coordinate is observed in the vicinity of product end (Axial = 1) where the O_2 adsorbed amount progressively increases from the centre to the surface of the micropore while the Ar adsorbed amount remains constant for more than half distance from the pore centre and then raises and diminishes exhibiting a maximum at Radial ≈ 0.9.

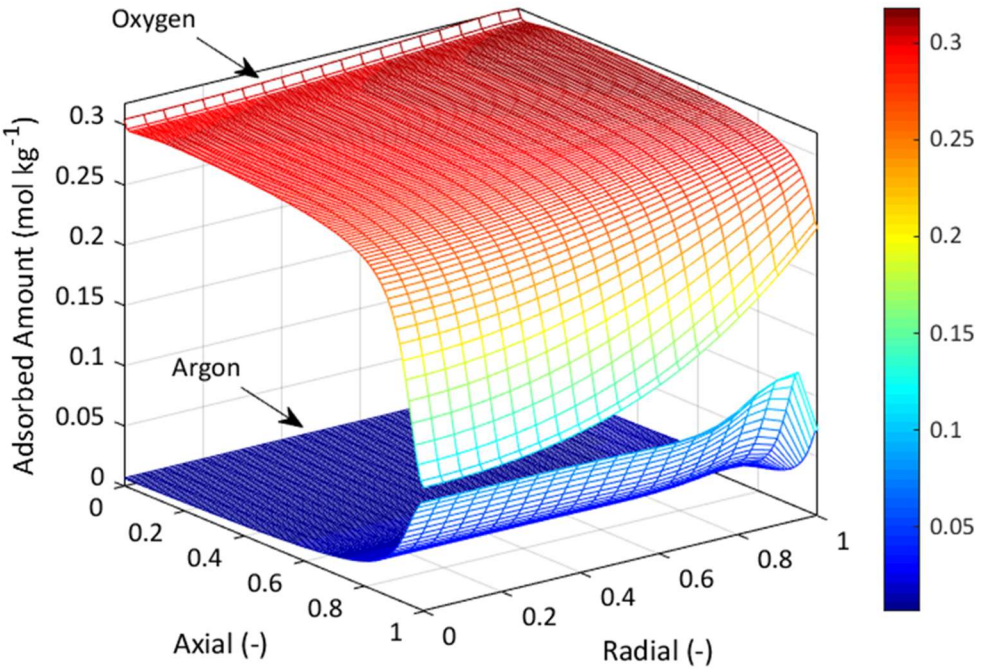

Figure 12. 3-D plots of Ar and O_2 adsorbed phase concentration along the dimensionless axial column distance and radial micropore distance at the end of adsorption step for Run 20. Simulation run information is reported in Table 6

Eventually, Figure 13 reports the O_2 average adsorbed phase concentration along the dimensionless axial column distance for Run 20 at the end of several steps of the VSA cycle. It can be noted how the profile drops significantly to an average value of 0.1 mol kg^{-1} at the end of blowdown step compared to adsorption and depressurizing pressure equalization steps, and then it gets further halved at the end of the self-purging step, thus confirming the efficacy of the self-purge.

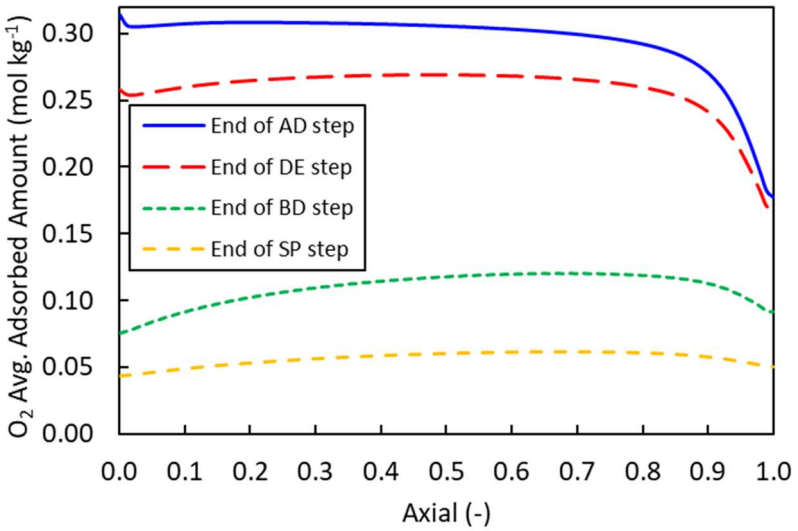

Figure 13. Profiles of O_2 average adsorbed phase concentration along the dimensionless axial column distance for Run 20 at the end of several steps of the VSA cycle. Simulation run information is reported in Table 6

4.5 Second-stage VSA Simulations

A second-stage VSA unit acting as an Ar purifier was designed in order to increase the argon purity from 50.8% to the 98+% specification. Given the best performance found for the first-stage, a 2-bed 6-step cycle configuration was selected for the second-stage with the same operational pressure swing of 0.1–1 bar. From the results obtained for Run 20 the raffinate molar flowrate feeding the second-stage unit was calculated as 1.23 mol s^{-1} (or 0.03 sm^3 s^{-1}). A list of column parameters as well as operating conditions used for the second-stage 2-bed VSA system can be found in Table 8.

Table 8. Column parameters and operating conditions of the second-stage 2-bed VSA system

Column parameters	
L_c (m)	3.2
D_c (m)	0.64
ε (-)	0.4
D_z (m^2 s^{-1})	1.4×10^{-3}
K_z (W m^{-1} K^{-1})	0.29
h_w (W m^{-2} K^{-1})	8.2
Operating conditions	
Feed composition (mol%)	50.8% Ar ; 49.2% O_2
Adsorption pressure (bar)	1.013
Desorption pressure (bar)	0.1
Feed temperature (K)	303.15
Molar feed flowrate (mol s^{-1})	1.23 (or 0.030 sm^3 s^{-1})
Volumetric feed flowrate (m^3 s^{-1})	0.031

Additional four simulation runs were carried out to assess the KPIs of the second-stage VSA system. The simulation results are summarized in Table 9. With the adsorption step time of 30 s Run 25 achieved an argon purity of 98.1% with a recovery of 39.8%, thus meeting the product purity requirements. As the feed to the second-stage VSA unit was already highly enriched with Ar the simulation runs showed bed productivities one order of magnitude higher and specific energy consumptions one order of magnitude lower than those of the first-stage VSA unit.

Connecting the two VSA processes in series (Run 20 + Run 25), the estimated overall performance was: argon purity of 98.1%, argon recovery of 20.3%, bed productivity of 0.011 mol_{Ar} kg_{ads}^{-1} h^{-1} and specific energy consumption of 53.2 MJ kg_{Ar}^{-1}. Since the calculations were

based on the total amount of Ar produced in the second-stage VSA unit, argon recovery, bed productivity and specific energy consumption of the integrated system resulted poorer than either of the two stages. The overall mass balance of the integrated two-stage process is shown in Figure 14. In the patent disclosed by Hayashi et al. [3] it was claimed that they concentrated argon to a purity of 99% with a recovery of 40% starting from a similar feed composition adsorbed on 3A CMS. Although the argon recovery reported in the patent is double than that of the present study the authors employed a much more complex apparatus equipped with four multi-bed VSA stages, two recycled streams, a catalytic deoxygenation unit, and operated the cycles with a maximum pressure swing between 0.13 and 3.5 bar. The proposed two-stage adsorptive argon concentration system is much simpler than that of the patent.

Table 9. Performance results of the second-stage 2-bed VSA system

Run #	*P_{ads} (bar)*	*P_{des} (bar)*	*t_{AD} (s)*	*Ar purity (%)*	*Ar recovery (%)*	*Bed productivity ($mol_{Ar}\ h^{-1}\ kg_{ads}^{-1}$)*	*Specific energy consumption ($MJ\ kg_{Ar}^{-1}$)*	*O_2 purity in offgas (%)*	*O_2 recovery in offgas (%)*
Run 25	1.013	0.1	30	98.1	39.8	0.34	2.24	61.5	99.2
Run 26			40	97.0	46.3	0.45	1.83	64.0	98.5
Run 27			50	95.4	51.6	0.56	1.57	66.1	97.4
Run 28			60	93.5	55.9	0.65	1.39	67.8	96.0

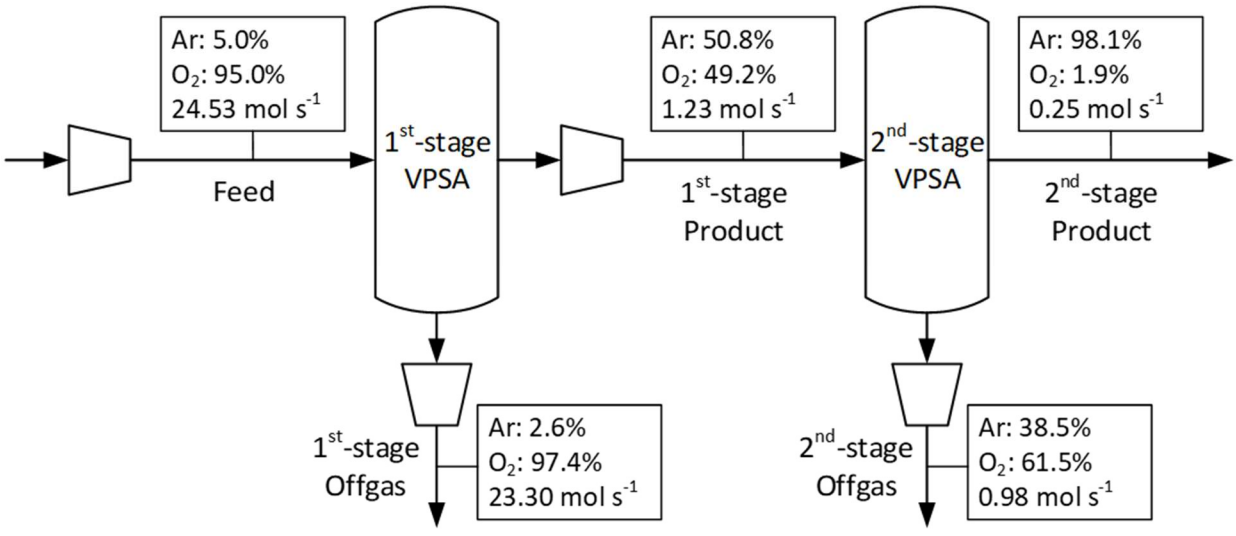

Figure 14: Overall mass balance of the two-stage VSA process for argon concentration

5. Techno-economic Comparison with Cryogenic Distillation

In the previous section the specific energy consumption associated with the two-stage VSA process for argon concentration was estimated as 53.2 MJ kg_{Ar}^{-1}. This figure could be

directly compared to the energy consumption of a conventional stand-alone cryogenic distillation unit applied to the same 95:5 mol% oxygen-argon feed. The process configuration was adapted from the single distillation column system designed for nitrogen production reported by Agrawal and Herron [1] with a modified multi-stream heat exchanger presented by Fu and Gundersen [11], and its operating conditions were adjusted for the new feed conditions. The resulting single-column cryogenic distillation process for argon concentration was simulated in gPROMS ProcessBuilder environment [48] with the flowsheet shown in Figure 15.

Given that the column has the overhead pressure of 10 bar, the feed is compressed from atmospheric pressure to 11.2 bar assuming 1 kPa of pressure drop per tray [58]. The feed is then cooled to 303.15 K in the cooler and further cooled to its dew point (123.0 K) in the main heat exchanger by exchanging heat against the returning streams. The pressure of 10 bar was selected in order to operate the main heat exchanger with a temperature difference of 2.5 K and a larger temperature difference in the reboiler-condenser. The cooled feed stream is then fed to the bottom of the refluxed distillation column where 120 equilibrium stages are used to attain the argon purity of 98.1% at the top of this column. A portion of the argon vapour from the top is withdrawn and partially warmed in the main heat exchanger and then expanded in the turbo-expander to a pressure near atmospheric pressure to provide the desired argon product. The major portion of the argon vapour stream is condensed in a reboiler-condenser and returned as reflux to the column with a molar reflux ratio close to 112. The crude liquid oxygen stream from the bottom of the column is reduced in pressure through the valve to a pressure near atmospheric pressure and vaporized in the reboiler-condenser. The vaporized stream is warmed in the main heat exchanger to provide the refrigeration needed for the plant. The concentration of oxygen in the offgas stream is approximately 95.9%.

Table 10 details the process specifications and the simulation results of the conventional stand-alone cryogenic distillation unit. Pressure drops were assumed negligible across the units in the flowsheet other than the distillation column. From Table 10 the specific energy consumption for the stand-alone cryogenic distillation process was 30.4 MJ kg_{Ar}^{-1}, which is 57.1% of that of the two-stage VSA process. However, the adsorptive-based unit was largely penalized by the low vacuum pump adiabatic efficiency of 40% that is exactly half of the compressor efficiency (80%) used in the cryogenic distillation-based unit.

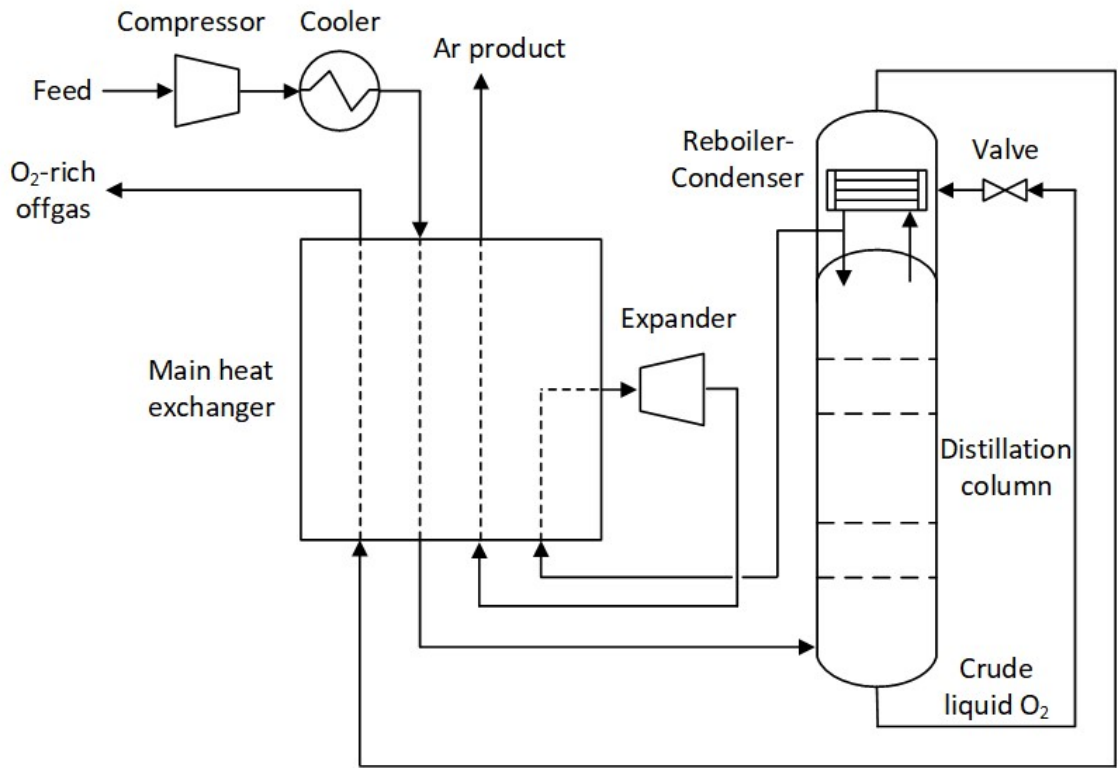

Figure 15: Process flowsheet of the conventional stand-alone cryogenic distillation unit for argon concentration

Table 10: Process specifications and simulation results of the conventional stand-alone cryogenic distillation unit for argon concentration

Process specifications	
Compressor pressure ratio (-)	11.1
Compressor isentropic efficiency (%)	80
Expander pressure ratio (-)	10
Expander isentropic efficiency (%)	80
Valve outlet pressure (bar)	1.1
Cooler outlet temperature (K)	303.15
Temperature difference in main heat exchanger (K)	2.5
Temperature difference in reboiler-condenser (K)	10
Column operating pressure (bar)	10
Column number of equilibrium stages (#)	120
Argon purity in distillate (%)	98.1
Simulation results	
Compressor power consumption (kW)	265.9
Expander power generation (kW)	0.3
Column molar reflux ratio (-)	112.2
Argon recovery in distillate (%)	17.8
Overall specific energy consumption (MJ kg_{Ar}^{-1})	30.4

At the same time it is worth noticing that the cryogenic distillation unit requires 120 equilibrium stages which will result in a more than 60 m tall column while the high reflux ratio will result in a large diameter as well. Compared to the VSA process, the cryogenic distillation will also incur greater costs of material of construction due to the need of larger thicknesses to handle the operating pressure of 10 bar and the use of stainless steels capable to withstand cryogenic temperatures.

This is in agreement with the results of a recent project carried out for the U.S. Department of Energy aiming to assess different technologies for oxygen production for energy systems [59]. The authors performed a comprehensive capital cost estimation of a cryogenic ASU for a large scale benchmark (400,000 $Nm^3 h^{-1} O_2$) and a VSA system for a small scale benchmark (2,500 $Nm^3 h^{-1} O_2$) which is very close to the Ar VSA system's capacity. It was reported that the fixed capital investment was $377 MM for the ASU and $4.43 MM for the VSA system. The capital cost of the ASU with a capacity scaled down to 2,500 $Nm^3 h^{-1}$ can be calculated using the six-tenths rule [60] as $17.9 MM, which is approximately four times greater than the VSA capital cost. Given the similar operating conditions it is anticipated that a comparable CAPEX ratio would also apply to the cryogenic distillation and the VSA system to concentrate argon. Therefore, it can be concluded that the VSA technology is a more attractive option in terms of unit CAPEX with also potential OPEX savings considering the parallel operation of multiple and more efficient vacuum pumps.

6. Conclusions

The aim of this work was to design an industrial (V)PSA process capable of concentrating and purifying argon up to 98+% from a 95:5 mol% oxygen-argon raffinate stream of a new-generation containerised O_2 VSA plant. A complete mathematical model coupling mass, energy and momentum balances was implemented to simulate the adsorption dynamics of the PSA system including the surrounding ancillary equipment. The kinetic separation on CMS adsorbent was described by the IAS theory coupled with the Langmuir model for the equilibrium and the concentration-dependent micropore diffusion model for the mass transfer.

Three different cycle configurations involving one, two and three beds were investigated considering operational pressure swings of 1–3 bar and 0.1–1 bar and varying the adsorption step time as well as the vacuum desorption pressure. It was shown that the VSA cycles performed considerably better than the PSA cycles in terms of argon purity and recovery, but at the expenses of loss of bed productivity and higher energy consumption. Against the stringent product purity requirement it was not possible to achieve an argon purity higher than 60% with an acceptable recovery using a single VSA unit; hence a second-stage VSA unit was also designed and simulated. The integrated VSA system included a 2-bed first-stage enriching-unit where the Ar purity was increased from 5.0% to 50.8% and a 2-bed second-

stage purification-unit where the purity raised up to 98.1%. The overall Ar recovery of this process was 20.3% with a bed productivity of 0.011 mol_{Ar} kg_{ads}^{-1} h^{-1} and a specific energy consumption of 53.2 MJ kg_{Ar}^{-1}.

As a result of the process simulation study, it was found that, with the same product purity, the integrated VSA process of this study had an energy consumption 75% higher than that of a conventional stand-alone cryogenic distillation-based process mainly due to the large difference in turbomachinery efficiency. However, the VSA technology is expected to exhibit a more favourable CAPEX than the cryogenic distillation due to the lower unit size and cheaper material of construction.

Nomenclature

A_c Column surface area (m^2)
b_i Equilibrium constant of component i (bar^{-1})
$b_{i,0}$ Pre-exponential equilibrium constant coefficient of component i (bar^{-1})
c_i Gas phase concentration of component i (mol m^{-3})
$c_{p,s}$ Particle specific heat capacity (J kg^{-1} K^{-1})
c_T Total gas phase concentration (mol m^{-3})
C_v Valve flow coefficient (kg s^{-1} $Pa^{-1/2}$)
D_c Column diameter (m)
D_i Micropore diffusivity of component i (m^2 s^{-1})
$D_{i,0}$ Micropore intrinsic mobility of component i (m^2 s^{-1})
D_m Molecular diffusivity (m^2 s^{-1})
d_P Particle diameter (m)
D_z Axial mass dispersion coefficient (m^2 s^{-1})
F Mass flowrate (kg s^{-1})
F_i Assigned mass flowrate (kg s^{-1})
$(-\Delta H_i)$ Heat of adsorption of component i (J mol^{-1})
H_g Gas phase enthalpy per unit volume (J m^{-3})
h_w Heat transfer coefficient between the gas phase and the column wall (W m^{-2} K^{-1})
J_i Diffusive flux of component i (mol m^{-2} s^{-1})
J_T Thermal diffusive flux (W m^{-2})
k_g Gas thermal conductivity (W m^{-1} K^{-1})
k_z Axial thermal dispersion coefficient (W m^{-1} K^{-1})
L_c Column length (m)
m_{ads} Adsorbent mass (kg)
MW_i Molecular weight of component i (kg mol^{-1})
P Pressure (bar)
ΔP Pressure difference (Pa)

P_{ads} Adsorption pressure (bar)

P_{atm} Atmospheric pressure (bar)

P_{des} Desorption pressure (bar)

P_i Partial pressure of component i (bar)

P_i^0 Surface pressure of component i (bar)

Pr Prandtl number (-)

q_i Adsorbed phase concentration of component i (mol kg^{-1})

q_i^* Adsorbed phase concentration of component i at equilibrium (mol kg^{-1})

$\overline{q}_i$ Averaged adsorbed phase concentration of component i in the particle (mol kg^{-1})

$q_{s,i}$ Saturation capacity of component i (mol kg^{-1})

q_T Total adsorbed phase concentration (mol kg^{-1})

R Ideal gas constant (J mol^{-1} K^{-1})

r Radial distance in the micropore (m)

r_c Micropore radius (m)

Re Reynolds number (-)

Sc Schimdt number (-)

t Time (s)

t_{cycle} Cycle time (s)

T Temperature (K)

T_w Column wall temperature (K)

u Interstitial velocity (m s^{-1})

U_g Gas phase internal energy per unit volume (J m^{-3})

U_s Particle internal energy per unit volume (J m^{-3})

V_{SP} Valve stem position (-)

w_i Gas phase mass fraction of component i (-)

x_i Adsorbed phase molar fraction of component i (-)

y_i Gas phase molar fraction of component i (-)

z Axial distance along the column (m)

Greek letters

γ Ratio of specific heat capacities c_p/c_v (-)

ε External bed void fraction (-)

η_c Compressor efficiency (-)

η_v Vacuum pump efficiency (-)

θ_i Fractional adsorption coverage of component i (-)

μ Gas viscosity (Pa s)

ρ_g Gas density (kg m^{-3})

ρ_s Particle density (kg m^{-3})

ψ_{eq} Reduced grand potential at equilibrium (mol kg^{-1})

ψ_i Reduced grand potential of component i (mol kg^{-1})

References

[1] Agrawal, R., Herron, D.M.: Air Liquefaction: Distillation. Encyclopedia of Separation Science, Academic Press, 1895–1910 (2000)

[2] Timmerhaus, K.D., Flynn, T.M.: Cryogenic Process Engineering. International Cryogenics Monograph Series, Springer Science+Business Media, New York (1989)

[3] Hayashi, S., Tsuchiya, H., Haruna, K.: Process for obtaining high concentration argon by pressure-swing-adsorption. US Patent 4529412 to Seitetsu Kagaku Co., Ltd. (1985)

[4] Prosser, N.M., Luo, Y.: Method and apparatus for argon recovery in a cryogenic air separation unit with a pressure swing adsorption. US Patent 10145609 B2 to Praxair Technology Inc. (2018)

[5] Wineaware: Wine Preservation Systems (2020). Available at https://www.wineware.co.uk/wine-preservation/wine-preservation-systems/

[6] Smith, A.R., Klosek, J.: A review of air separation technologies and their integration with energy conversion processes. Fuel Processing Technology 70, 115–134 (2001)

[7] Linde: Air separation plants. History and technological progress in the course of time (2019). Available at https://www.linde-engineering.com/en/images/Air-separation-plants-history-and-technological-progress-2019_tcm19-457349.pdf

[8] Zhong, G., Baksh, M.S.A., Notaro, F., Leavitt, F.W.: Pressure swing adsorption process for high recovery of high purity gas. US Patent 6500235 B2 to Praxair Technology Inc. (2002)

[9] Kovak, K.W., Agrawal, R., Peterson, J.C.: Method for purifying argon through cryogenic adsorption. US Patent 5159816 to Air Products and Chemicals, Inc. (1992)

[10] Cornelissen, R.L., Hirs, G.G.: Exergy analysis of cryogenic air separation. Energy Conversion and Management 39, 1821–1826 (1998)

[11] Fu, C., Gundersen, T.: Using exergy analysis to reduce power consumption in air separation units for oxy-combustion processes. Energy 44, 60–68 (2012)

[12] Fu, C., Gundersen, T.: Recuperative vapour recompression heat pumps in cryogenic air separation processes. Energy 59, 708–718 (2013)

[13] Aneke, M., Wang, M.: Potential for improving the energy efficiency of cryogenic air separation unit (ASU) using binary heat recovery cycles. Applied Thermal Engineering 81, 223–231 (2015)

[14] Kumar, R., Sircar, S., White, T.R., Greskovich, E.J.: Argon purification. US Patent 4477265 to Air Products and Chemicals, Inc. (1984)

[15] Howard, H.E., Kechagia, P.E., Barrett, P.A., Handley, J.R.: Argon production method and apparatus. US Patent 9644890 B2 to Praxair Technology, Inc. (2017)

[16] Air Liquide: Technology Handbook (2018). Available at https://www.engineering-airliquide.com/sites/activity_eandc/files/2018/03/28/air-liquide-technology-handbook-march-2018.pdf

[17] Hayashi, S., Kawai, M., Kaneko, T.: Dynamics of high purity oxygen PSA. Gas Separation and Purification 10, 19–23 (1996)

[18] Luberti, M., Oreggioni, G.D., Ahn, H.: Design of a rapid vacuum pressure swing adsorption process for post-combustion CO_2 capture from a biomass-fuelled CHP plant. Journal of Environmental Chemical Engineering 5: 3973–3982 (2017)

[19] Yang, R.T.: Gas separation by adsorption processes. Butterworths, Boston (1987)

[20] Anson, A., Kuznicki, S.M., Kuznicki, T., Dunn, B.C., Eyring, E.M., Hunter, D.B.: Separation of argon and oxygen by adsorption on a titanosilicate molecular sieve. Separation Science and Technology 44, 1604–1620 (2009)

[21] Kim, M.-B., Jee, J.-G., Bae, Y.-S., Lee, C.-H.: Parametric study of pressure swing adsorption process to purify oxygen using carbon molecular sieve. Ind. Eng. Chem. Res. 44, 7208–7217 (2005)

[22] Santos, J.C., Cruz, P., Regala, T., Magalhaes, F.D., Mendes, A.: High-purity oxygen production by pressure swing adsorption. Ind. Eng. Chem. Res. 46, 591–599 (2007)

[23] Shi, M., Kim, J., Sawada, J.A., Lam, J., Sarabadan, S., Kuznicki, T.M., Kuznicki, S.M.: Production of argon free oxygen by adsorptive air separation on Ag-ETS-10. AIChE Journal 59, 982–987 (2013)

[24] Knaebel, K.S., Kandybin A.: Pressure swing adsorption system to purify oxygen. US Patent 5226933 to Ohio State University (1993)

[25] Kandybin, A.I., Anderson, R.A., Reichley, D.L.: System for separation of oxygen from argon/oxygen mixture. US Patent 5470378 to Arbor Research Corporation (1995)

[26] Dee, D.P., Chiang, R.L., Miller, E.J., Whitley, R.D.: High purity oxygen production by pressure swing adsorption. US Patent 6544318 B2 to Air Products and Chemicals, Inc. (2003)

[27] Ma, Y.H., Sun, W., Bhandarkar, M., Wang, J., Miller, G.W.: Adsorption and diffusion of nitrogen, oxygen, argon, and methane in molecular sieve carbon at elevated pressures. Separations Technology 1, 90–98 (1991)

[28] Reid, C.R., O'koye, I.P., Thomas, K.M.: Adsorption of gases on carbon molecular sieves used for air separation. Langmuir 14, 2415–2425 (1998)

[29] Huang, Q., Sundaram, S.M., Farooq, S.: Revisiting transports of gases in micropores of carbon molecular sieves. Langmuir 19, 393–405 (2003)

[30] Rege, S.U., Yang, R.T.: Kinetic separation of oxygen and argon using molecular sieve carbon. Adsorption 6, 15–22 (2000)

[31] Jin, X., Malek, A., Farooq, S.: Production of argon from an oxygen–argon mixture by pressure swing adsorption. Ind. Eng. Chem. Res. 45, 5775–5787 (2006)

[32] Linde: Oxygen generation. By Vacuum Pressure Swing Adsorption (2017). Available at https://www.linde-engineering.com/en/images/Oxygen%20generation.%20By%20Vacuum%20Pressure%20Swing%20Adsorption._tcm19-416454.pdf

[33] Hassan, M.M., Raghavan, N.S., Ruthven, D.M.: Pressure swing air separation on a carbon molecular sieve – II. Investigation of a modified cycle with pressure equalization and no purge. Chemical Engineering Science 42, 2037–2043 (1987)

[34] Ruthven, D.M., Farooq, S., Knaebel, K.S.: Pressure swing adsorption. VCH Publishers, New York (1994)

[35] Kikkinides, E.S., Yang, R.T.: Concentration and recovery of CO_2 from flue gas by Pressure Swing Adsorption. Ind. Chem. Eng. Res. 32, 2714–2720 (1993)

[36] Luberti, M., Friedrich, D., Brandani, S., Ahn, H.: Design of a H_2 PSA for cogeneration of ultrapure hydrogen and power at an advanced integrated gasification combined cycle with pre-combustion capture. Adsorption 20, 511–524 (2014)

[37] Luberti, M., Kim, Y.-H., Lee, C.-H., Ferrari, M.-C., Ahn H.: New momentum and energy balance equations considering kinetic energy effect for mathematical modelling of a fixed bed adsorption column. Adsorption 21, 353–363 (2015)

[38] Ergun, S.: Fluid flow through packed columns. Chem. Eng. Prog. 48, 89–94 (1952)

[39] Myers, A.L., Prausnitz, J.M.: Thermodynamics of mixed-gas adsorption. AIChE Journal 11, 121–127 (1965)

[40] Santori, G., Luberti, M.: Thermodynamics of thermally-driven adsorption compression. Sustainable Materials and Technologies 10, 1–9 (2016)

[41] Ruthven, D.M., Raghavan, N.S., Hassan, M.M.: Adsorption and diffusion of nitrogen and oxygen in a carbon molecular sieve. Chemical Engineering Science 41, 1325–1332 (1986)

[42] Ruthven, D.M.: Diffusion of oxygen and nitrogen in carbon molecular sieve. Chemical Engineering Science 47, 4305–4308 (1992)

[43] Farooq, S., Ruthven, D.M.: Numerical simulation of a kinetically controlled pressure swing adsorption bulk separation process based on a diffusion model. Chemical Engineering Science 46, 2213-2224 (1991)

[44] Khalighi, M., Farooq, S., Karimi, I.A.: Optimizing the PSA process of propylene/propane using Neuro-Fuzzy modelling. Proceedings of the 11th International Symposium on Process Systems Engineering, 1336–1340 (2012)

[45] Chihara, K., Suzuki, M., Kawazoe, K.: Adsorption rate on molecular sieving carbon by chromatography. AIChE Journal 24, 237–246 (1978)

[46] Wakao, N., Funazkri, T.: Effect of fluid dispersion coefficients on particle-to-fluid mass transfer coefficients in packed beds. Chemical Engineering Science 33, 1375–1384 (1978)

[47] Specchia, V., Baldi, G., Sicardi, S.: Heat transfer in packed bed reactors with one phase flow. Chemical Engineering Communications 4, 361–380 (1980)

[48] Process System Enterprise Ltd (2020). Available at https://www.psenterprise.com/

[49] Liu, Z., Grande, C.A., Li, P., Yu, J., Rodrigues, A.E.: Multi-bed vacuum pressure swing adsorption for carbon dioxide capture from flue gas. Separation and Purification Technology 81, 307–317 (2011)

[50] Jain, S., Moharir, A.A., Li, P., Wozny, G.: Heuristic design of pressure swing adsorption: a preliminary study. Separation and Purification Technology 33, 25–43 (2003)

[51] Baksh, M.S.A., Rosinski, A.C.: Continuous feed three-bed pressure swing adsorption system. US Patent 7179324 B2 to Praxair Technology, Inc. (2007)

[52] Ebner, A.D., Mehrotra, A., Ritter, J.A.: Graphical approach for complex PSA cycle scheduling. Adsorption 15, 406–421 (2009)

[53] Keefer, B.G., McLean, C.R., Brown, M.J.: Electrical current generation system. US Patent 6921597 B2 to QuestAir Technologies Inc. (2005)

[54] Jee, J.-G., Kim, M.-B., Lee, C.-H.: Pressure swing adsorption processes to purify oxygen using a carbon molecular sieve. Chemical Engineering Science 60, 869–882 (2005)

[55] Edwards Ltd: Liquid ring vacuum pumps for the process industries (2020). Available at https://www.edwardsvacuum.com/en/our-products/liquid-ring-pumps

[56] Krishnamurthy, S., Rao, V.R., Guntuka, S., Sharratt, P., Haghpanah, R., Rajendran, A., Amanullah, M., Karimi, I.A., Farooq, S.: CO_2 capture from dry flue gas by vacuum swing adsorption: A pilot plant study. AIChE Journal 60, 1830–1842 (2014)

[57] Sun, L.M., Le Quere', P., Levan, M.D.: Numerical simulation of diffusion-limited PSA process models by finite difference methods. Chemical Engineering Science 51, 5341–5352 (1996)

[58] Treybal, R.E.: Mass-transfer operations, 3rd Edition. McGraw-Hill, Singapore (1981)

[59] Sethi, V.K., Lin, J., Deng, S., Targett, M.: Sorbent-based Oxygen Production for Energy Systems. United States (2017). Available at: https://doi.org/10.2172/1352448

[60] Sinnott, R., Towler, G.: Chemical Engineering Design, 5th Edition. Butterworth-Heinemann, Oxford (2009)